Isoquercitrin protects HUVECs against high glucose-induced apoptosis through regulating p53 proteasomal degradation

LIBO LIU[1,2*], SIHUI HUANG[1,2*], MAN XU[1,2], YAN GONG[3], DAN LI[1,2], CHUNXIA WAN[1,2], HAIMING WU[1,2] and QIZHU TANG[1,2]

[1]Department of Cardiology, Renmin Hospital of Wuhan University; [2]Hubei Key Laboratory of Metabolic and Chronic Diseases, Wuhan University, Wuhan, Hubei 430060; [3]Pharmacy Department, Union Hospital, Tongji Medical College, Huazhong University of Science and Technology, Wuhan, Hubei 430022, P.R. China

Received November 24, 2020; Accepted April 12, 2021

DOI: 10.3892/ijmm.2021.4955

Abstract. High glucose (HG)-induced endothelial apoptosis serves an important role in the vascular dysfunction associated with diabetes mellitus (DM). It has been reported that isoquercitrin (IQC), a flavonoid glucoside, possesses an anti-DM effect, but the mechanism requires further investigation. The present study investigated the effect of IQC against HG-induced apoptosis in human umbilical vein endothelial cells (HUVECs) and explored its molecular mechanism. HUVECs were treated with 5 or 30 mM glucose for 48 h. Endothelial cell viability was monitored using the Cell Counting Kit-8 assay. Mitochondrial membrane potential was detected by JC-1 staining. Apoptosis was observed by TUNEL staining and flow cytometry. Western blotting was used for the analysis of apoptosis-associated proteins Bax, Bcl-2, cleaved (C)-caspase3, total-caspase3, p53 and phosphorylated p53. Reverse transcription-quantitative PCR was used to analyze the mRNA expression levels of Bax, Bcl-2 and p53. Immunofluorescence staining was utilized to detect the expression levels and distribution of p53 and ubiquitin specific peptidase 10 (USP10) in HUVECs. The results revealed that IQC significantly attenuated HG-induced endothelial apoptosis, as shown by decreased apoptotic cells observed by TUNEL, JC-1 staining and flow cytometry. Moreover, under HG stress, IQC treatment markedly inhibited the increased expression levels of the pro-apoptotic proteins p53, Bax and C-caspase3, and increased the expression levels of the anti-apoptotic protein Bcl-2 in HUVECs. However, the anti-apoptotic effect of IQC against HG was partially blunted by increasing p53 protein levels *in vitro*. IQC influenced the mRNA expression levels of Bax and Bcl-2 in response to HG, but it did not affect the transcription of p53. Notably, IQC inhibited the HG-induced phosphorylation of p53 at Ser15 and the nuclear transport of USP10, destabilizing p53 and increasing the proteasomal degradation of the p53 protein. The current findings revealed that IQC exerted a protective effect against the HG-induced apoptosis of endothelial cells by regulating the proteasomal degradation of the p53 protein, suggesting that IQC may be used as a novel therapeutic compound to ameliorate DM-induced vascular complications.

Correspondence to: Professor Qizhu Tang, Department of Cardiology, Renmin Hospital of Wuhan University, 238 Jiefang Road, Wuhan, Hubei 430060, P.R. China
E-mail: qztang@whu.edu.cn

*Contributed equally

Abbreviations: IQC, isoquercitrin; HG, high glucose; DM, diabetes mellitus; HUVECs, human umbilical vein endothelial cells; RT-qPCR, reverse transcription-quantitative PCR; CCK-8, Cell Counting Kit-8; C/T-caspase 3, cleaved/total caspase 3; USP10, ubiquitin specific peptidase 10; MDM2, murine double minute 2

Key words: IQC, apoptosis, HG, endothelial cell, p53

Introduction

Diabetes mellitus (DM) is a common endocrine metabolic disorder with important features of hyperglycemia and glucose intolerance that have a long-lasting negative impact on humans (1). Vascular dysfunction in the heart and numerous other organs is a chronic complication of DM, and the crux of the vascular pathological state is endothelial dysfunction, which is associated with hyperactive immune responses, metabolic disturbances and abnormal vasoconstriction (2). The mechanism of DM-induced endothelial injury is complicated. It is currently accepted that apoptosis, oxidative stress and the inflammatory response account for DM-induced vascular damage. Apoptosis directly leads to endothelial cell death, thus playing a vital role in modulating endothelial function (3). Furthermore, a number of studies have confirmed that the excessive apoptosis of endothelial cells is closely associated with the pathological process of DM (4,5). Thus, inhibiting apoptosis-associated endothelial dysfunction may ameliorate DM-induced vascular complications (6-8). The association between high glucose (HG) stimulation and endothelial apoptosis has been extensively studied (9-11), as HG is a typical characteristic of DM.

Isoquercitrin (quercetin-3-O-β-D-glucopyranoside; IQC), a flavonoid glucoside, is widely distributed among medicinal herbs, fruit and vegetables. IQC has multiple protective effects against DM, cardiovascular disorders and vascular disease (12).

For instance, our previous study has proven that IQC decreases excessive inflammatory responses and enhances fatty acid oxidation to attenuate septic myocardial dysfunction (13). Similarly, IQC regulates the TLR4-mediated inflammatory signaling pathway to improve myocardial infarction in a rat model (14). In addition, IQC has been found to control the mesenteric arterial potassium channel state and endothelial nitric oxide level, consequently inducing vasodilation (15). A clinical study has shown that acute administration of IQC significantly improves endothelial function in volunteers at risk of cardiovascular disease (16). The aforementioned studies suggest that IQC can regulate endothelial function under pathological processes. Recently, a study of DM in a rat model has demonstrated that IQC can inhibit the oxidative stress, hyperlipidemia and inflammatory response in the liver, kidney and pancreas in rats treated with streptozotocin (17). However, the aforementioned study only showed results at the tissue level, and it is difficult to determine which cells were involved in this process.

Given the protective effect of IQC against DM in endothelial cells and the unknown effect of IQC on endothelial dysfunction induced by HG, the present study aimed to perform extensive experiments in HUVECs to investigate the effect of IQC in HG-treated HUVECs and explore its molecular mechanism.

Materials and methods

Chemicals and antibodies. Isoquercitrin (purity >98%) was obtained from Shanghai Winherb Medical Technology Co., Ltd. Primary antibodies against Bax (cat. no. 2772), Bcl-2 (cat. no. 2870), C-caspase 3 (cat. no. 9661), T-caspase 3 (cat. no. 9662P), p53 (cat. no. 2524), phosphorylated (p)-p53 (Ser15; cat. no. 9284) and GAPDH (cat. no. 2118) were purchased from Cell Signaling Technology, Inc. Ubiquitin specific peptidase 10 (USP10) antibody was purchased from ProteinTech Group, Inc. (cat. no. 19374-1-AP). Pifithrin-β and Nutlin-3 were obtained from MedChemExpress. USP10 small interfering (si)RNA and negative control (NC) siRNA were purchased from Sangon Biotech Co., Ltd., and adenovirus (ad)USP10 and adGFP were purchased from OBiO Technology (Shanghai) Corp., Ltd.

Endothelial cell culture and treatment. The immortal HUVEC cell line was purchased from YRGene (cat. no. NC006). The cells were grown in DMEM (cat. no. C11995) containing 10% FBS and 1% penicillin-streptomycin solution (cat. no. 15140) (all Gibco; Thermo Fisher Scientific, Inc.) under standard conditions (5% CO_2 and 37˚C). Before the experiment, cells were grown to 70-80% confluence and then synchronized in DMEM with 0.5% FBS for 12 h. Next, the cells were cultured with 10% FBS containing high D-glucose (30 mM; HG medium) or normal D-glucose (5 mM; NG medium) plus L-glucose (25 mM) to avoid the effects of osmotic imbalance in the cells as previously described (18-20). IQC (10, 50 or 100 μM) dissolved in PBS was added to NG or HG medium.

To inhibit p53 in cells exposed to glucotoxicity, the potent p53 inhibitor pifithrin-β (40 μM) was dissolved in DMSO (0.1% v/v) (21) and added to HUVECs stimulated with HG at 37˚C for 24 h. For p53 activation, Nutlin-3 (5 μM) dissolved in DMSO (0.1% v/v), which can effectively inhibit the interaction of murine double minute 2 (MDM2)-p53 and therefore activate p53 (22), was added to HUVECs treated with HG in the presence of IQC (100 μM) at 37˚C for 24 h.

Cell viability assay. To determine the cytotoxicity of IQC, the viability of HUVECs was tested using the Cell Counting Kit-8 (CCK-8) assay (Dojindo Molecular Technologies, Inc.). HUVECs were seeded in 96-well plates and treated with different concentrations of IQC (0, 2.5, 10, 50, 100, 200, 300 or 500 μM) in NG medium (5 mM) for 24 h at 37˚C. Subsequently, CCK-8 (10 μM) was added and incubated at 37˚C for 4 h. The absorbance rate was measured at 450 nm using a microplate reader (Synergy HT; Agilent Technologies, Inc.).

Measurement of mitochondrial membrane potential. Mitochondrial membrane potential was measured using the fluorescent JC-1 dye (Beyotime Institute of Biotechnology). Briefly, cells were grown in 6-well plates and treated with HG medium or NG medium with or without of IQC (10, 50 or 100 μM) at 37˚C for 48 h. After the different treatments, the cells were incubated with 10 mM JC-1 for 20 min at 37˚C in the dark, and then monitored using a fluorescence microplate microscope (magnification, x200) (Eclipse 80i; Nikon Corporation) at 529 nm (monomeric form of JC-1, green) and at 590 nm (aggregate form of JC-1, red).

TUNEL staining. Cells were plated in 24-well plates and treated with HG medium or NG medium with or without IQC (10, 50 or 100 μM) at 37˚C for 24 h. Subsequently, the cells were fixed in 4% paraformaldehyde for 10 min at room temperature and then apoptotic cells were detected using an ApopTag® Plus Fluorescein *In Situ* Apoptosis Detection kit (EMD Millipore) according to the manufacturer's protocol. After the TUNEL assay treatment, images were captured under an Olympus DX51 fluorescence microscope (magnification, x400) (Olympus Corporation).

Flow cytometry for apoptosis detection. Apoptosis was detected using an Annexin V-FITC/PI Apoptosis kit (cat. no. 556547; BD Biosciences). Cells were seeded in 6-well plates and treated with HG medium or NG medium with or without IQC (100 μM) at 37˚C for 24 h. Subsequently, the cells were washed with cold PBS and resuspended in 1X binding buffer at a concentration of $1x10^6$ cells/ml. Annexin V-FITC and PI were added and incubated at room temperature for 15 min according to the manufacturer's instructions. Finally, the samples were analyzed by flow cytometry (CytoFLEX; Beckman Coulter, Inc.) within 1 h, and then the data were analyzed using CytExpert 2.0 (Beckman Coulter, Inc.).

Immunofluorescence staining and confocal laser scanning microscopy. Cells were fixed in 4% paraformaldehyde at room temperature for 10 min and permeabilized in 0.2% Triton X-100. Subsequently, 10% goat serum albumin (Invitrogen; Thermo Fisher Scientific, Inc.) was used to block the cells at room temperature for 1 h. The cells were incubated in a solution containing diluted anti-p53 (1:100) with or without anti-USP10 (1:100) overnight at 4˚C and incubated with Alexa Fluor 488 (green) fluorescent secondary antibodies (1:200) at room temperature for 1 h

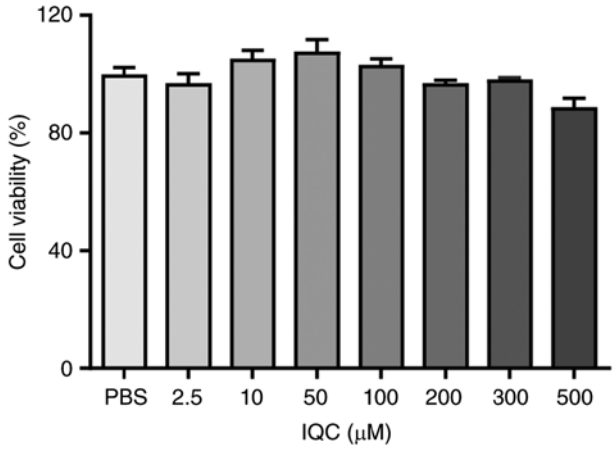

Figure 1. Cell viability of HUVECs treated with IQC. The cytotoxicity of IQC (0, 2.5, 10, 50, 100, 200, 300 and 500 μM) in HUVECs was assessed using the Cell Counting Kit-8 assay (n=6 for each group). IQC, isoquercitrin; HUVECs, human umbilical vein endothelial cells.

(cat. no. A11008; Invitrogen; Thermo Fisher Scientific, Inc.). The nuclei were counterstained with DAPI at room temperature for 1 min. Images were captured under an Olympus DX51 fluorescence microscope (Olympus Corporation) (magnification, x400) or an Olympus FV1200 confocal laser scanning microscope (magnification, x1,000) (Olympus Corporation).

Reverse transcription-quantitative PCR (RT-qPCR). Total RNA was extracted from HUVECs using TRIzol® reagent (cat. no. 15596-026; Invitrogen; Thermo Fisher Scientific, Inc.) and reverse transcribed to cDNA with a Transcriptor First Strand cDNA Synthesis kit (cat. no. 04896866001; Roche Diagnostics), according to the manufacturer's instructions. Subsequently, Light Cycler 480 SYBR Green Master Mix (cat. no. 04887352001; Roche Diagnostics) was used for qPCR analysis, according to the manufacturer's instructions. PCR thermocycling conditions were as follows: Initial denaturation at 95˚C for 10 min, followed by 40 cycles of 95˚C for 15 sec, 60˚C for 5 sec and 72˚C for 15 sec. Data were analyzed using the $2^{-\Delta\Delta Cq}$ method (23). The following primer sequences were used: Bax forward, 5'-TCATGGGCTGGACATTGGAC-3' and reverse, 5'-GCGTCCCAAAGTAGGAGAGG-3'; Bcl-2 forward, 5'-AACATCGCCCTGTGGATGAC-3' and reverse, 5'-GACTTCACTTGTGGCCCAGAT-3'; p53 forward, 5'-AAGTCTAGAGCCACCGTCCA-3' and reverse, 5'-CAATCCAGGGAAGCGTGTCA-3'; and GAPDH forward, 5'-CATCACCATCTTCCAGGAGCGAGA-3' and reverse, 5'-TGCAGGAGGCATTGCTGATGATCT-3'. The mRNA expression levels of Bax, Bcl-2 and p53 were normalized to those of GAPDH.

Western blotting. Western blotting was used to detect the protein expression levels of Bax, Bcl-2, C-caspase 3, T-caspase 3, p-p53, p53 and GAPDH. Briefly, cells were lysed with RIPA lysis buffer, and then protein concentrations were evaluated using a BCA protein assay kit (cat. no. 23227; Thermo Fisher Scientific, Inc.). Total protein (50 μg/lane) was electrophoresed using 10-12% SDS-PAGE and transferred onto PVDF membranes. The membranes were blocked with 5% milk and 0.1% Tween-20 in 1X TBS for 1 h at room temperature with gentle shaking, and then incubated overnight at 4˚C with primary antibodies (1:1,000) against Bax, Bcl-2, C-caspase 3, T-caspase 3, p-p53, p53 and GAPDH. After incubation with horseradish peroxidase-conjugated secondary antibodies (1:10,000; cat. no. A21020; Abbkine Scientific Co., Ltd.) at 37˚C for 1 h, the immunoblots were detected with ECL reagents and scanned using the Odyssey Infrared Imaging System (LI-COR Biosciences). Densitometry was analyzed using Image Lab software (v3.0; Bio-Rad Laboratories, Inc.).

USP10 gene silencing and overexpression. To knock down USP10 expression, HUVECs were seeded in 6-well plates, grown in antibiotic-free HG medium for 48 h and then transfected with USP10 siRNA (siUSP10; position 1583-1601; 5'-CCACCTGATGAAGTTCATT-3') and non-targeting NC siRNA using Lipofectamine® 6000 (Beyotime Institute of Biotechnology) at a final concentration of 100 nM at 37˚C for 6 h according to the manufacturer's instructions. The medium was then replaced with fresh culture medium with or without IQC (100 μM) for another 48 h at 37˚C before subsequent experiments.

For overexpression of USP10, the adenovirus-mediated overexpression system containing full-length USP10 cDNA (adUSP10) and the NC adenovirus vector (adGFP) were used. Cells were infected with adUSP10 or adGFP at a multiplicity of infection (MOI) of 50 at 37˚C for 24 h according to the manufacturer's instructions, and then the medium was replaced with fresh culture medium with or without IQC (100 μM) at 37˚C for another 48 h before subsequent experiments. The efficiency of USP10 siRNA and adUSP10 was assessed by western blotting, as aforementioned.

Statistical analysis. All experiments were repeated at least three times. Images were quantified using Image-Pro Plus 6.0 software (Media Cybernetics, Inc.). Data are presented as the mean ± SEM and were analyzed using SPSS 24.0 software (IBM Corp.). Normal distribution detection was determined using a one-sample Kolmogorov-Smirnov test. Differences between groups were analyzed by one-way ANOVA and Tukey's post-hoc test if the data were homoscedastic. Alternatively, Tamhane's T2 test was used. $P<0.05$ was considered to indicate a statistically significant difference.

Results

Effects of IQC on endothelial cell survival. To evaluate whether IQC affected the survival of HUVECs during the experiments, HUVECs were treated with 0, 2.5, 10, 50, 100, 200, 300 or 500 μM IQC in NG medium for 24 h. The CCK-8 assay results revealed that at concentrations of 2.5, 10, 50 or 100 μM IQC did not affect the viability of HUVECs, while the higher concentrations of IQC (200, 300 and 500 μM) slightly decreased cell viability (Fig. 1). No significant differences in cell viability were observed among these groups. Thus, 10, 50 and 100 μM IQC were chosen for subsequent experiments.

IQC protects HUVECs against HG-induced apoptosis. Since apoptosis serves an important role in HG-induced injury, the effect of IQC on the apoptosis of endothelial cells was examined. First, apoptosis was analyzed through TUNEL

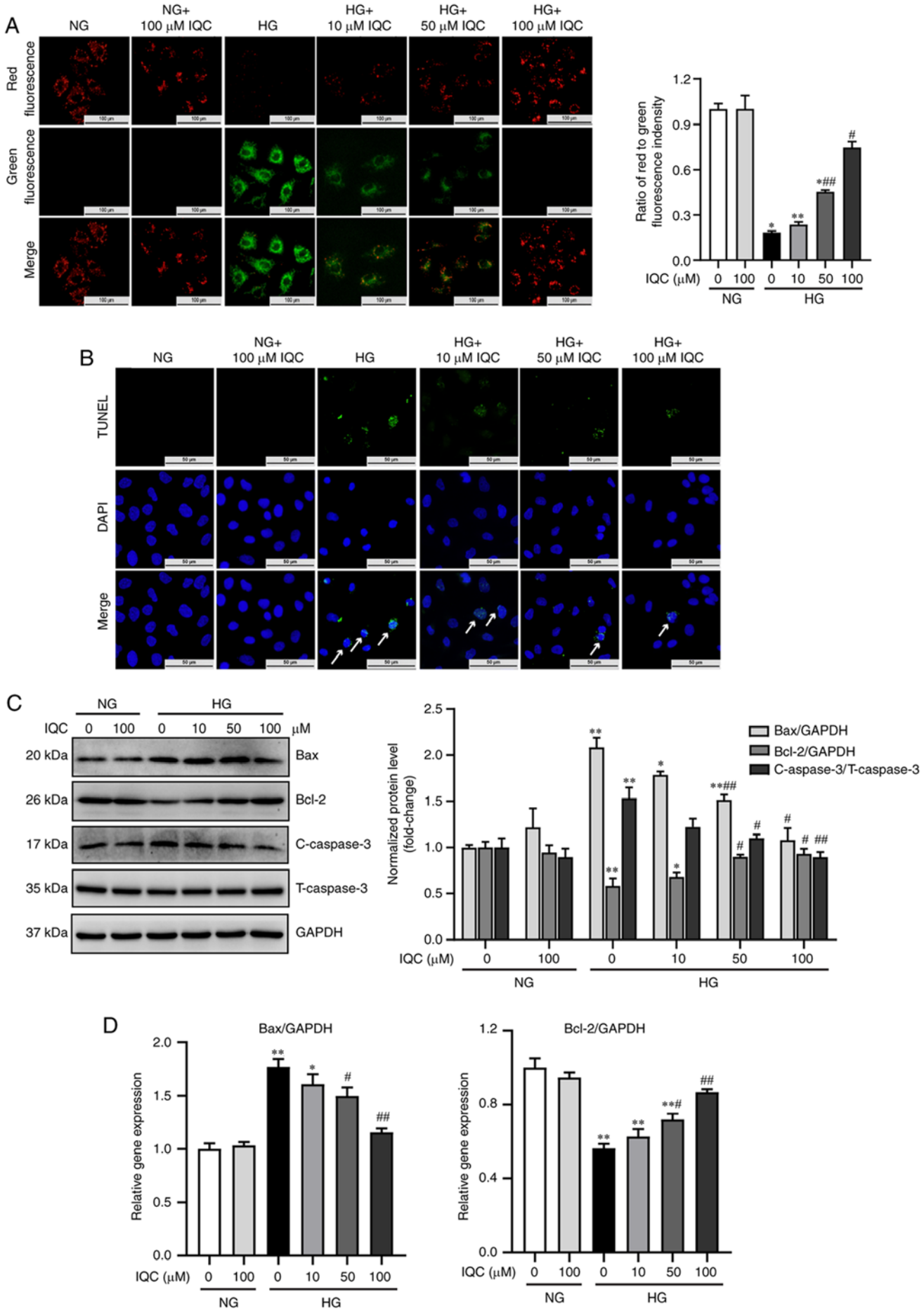

Figure 2. Continued.

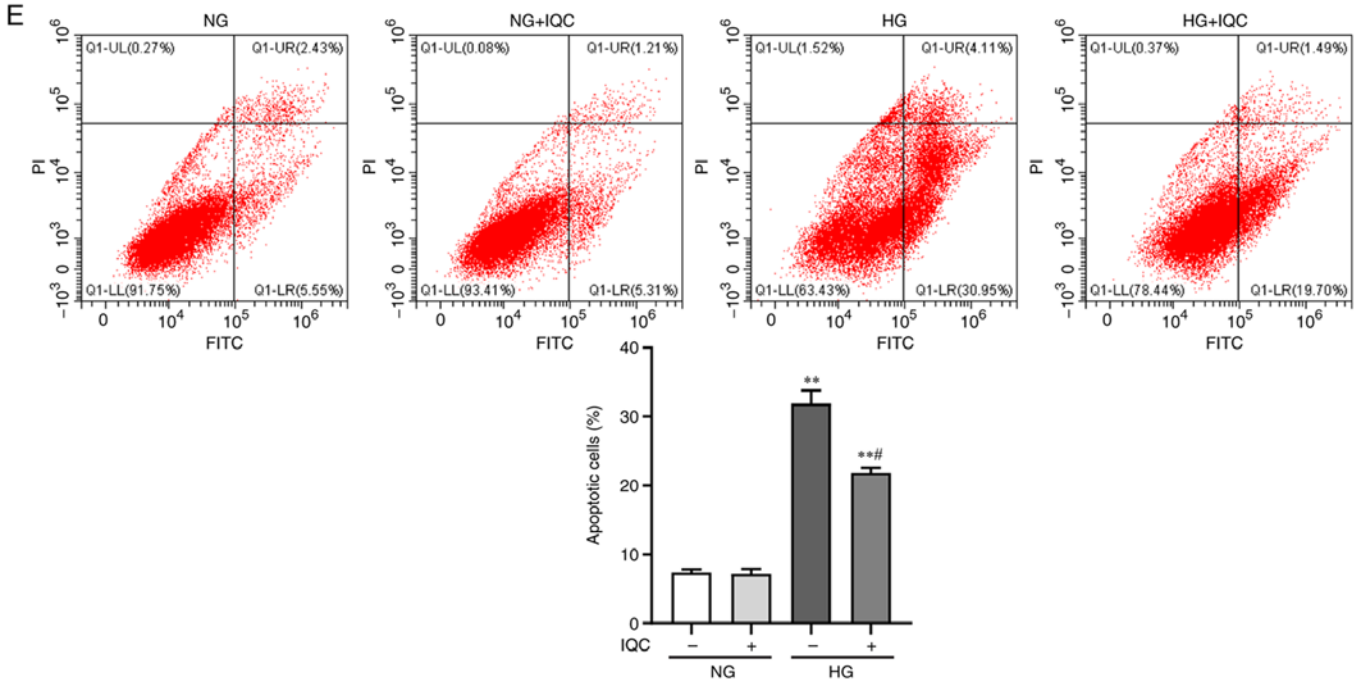

Figure 2. IQC attenuates the HG-induced apoptosis of HUVECs. (A) Representative images of JC-1 staining were used to observe the change in mitochondrial membrane potential in the indicated groups, and the ratio of red fluorescence to green fluorescence was quantified. Scale bar, 100 μm. (B) TUNEL assay was used to assess apoptosis levels by fluorescence microscopy in different groups. TUNEL positive cells (green); nucleus/DAPI (blue). Arrows indicate apoptotic cells. Scale bar, 50 μm. (C) Representative western blotting images of Bax, Bcl-2, C-caspase3, T-caspase3 and GAPDH protein bands and their quantification in the indicated groups (n=3). GAPDH was used as a control. (D) Relative mRNA expression levels of Bax and Bcl-2 in HUVECs in each group with different treatments (n=6). GAPDH was used as a control. (E) Representative dot plots of the apoptosis rate as measured by flow cytometry after AnnexinV-FITC/PI staining and quantitative data of the percentage of apoptotic cells (n=3). *P<0.05 and **P<0.01 vs. NG. $^{\#}$P<0.05 and $^{\#\#}$P<0.01 vs. HG. NG, normal glucose; HG, high glucose; IQC, isoquercitrin; HUVECs, human umbilical vein endothelial cells; C/T-caspase 3, cleaved/total caspase 3.

staining. TUNEL positive cells (green) were considered as apoptotic cells. As shown in Fig. 2B, the number of green spots in HUVECs was markedly increased under HG stress. When HUVECs were treated with 10, 50 or 100 μM IQC and HG, the green spots were markedly decreased (Fig. 2B). To further confirm the anti-apoptotic effect of IQC, JC-1 staining was used to examine the mitochondrial membrane potential. Green fluorescence indicates depolarized mitochondrial membrane potential, while red fluorescence indicates normal mitochondrial membrane potential. The ratio of red fluorescence to green fluorescence represents the degree of mitochondrial depolarization. To some extent, a decreased fluorescence ratio indicates increased apoptosis. The present results revealed that HG resulted a significant decrease in the fluorescence ratio in HUVECs compared with NG (Fig. 2A). By contrast, the ratio gradually increased after treatment with IQC (Fig. 2A). Furthermore, Annexin V-FITC/PI staining was used to investigate the effects of IQC on apoptosis stimulated by HG. The apoptotic rates in the NG, NG+IQC, HG and HG+IQC groups were 7.350±0.457, 7.163±0.709, 31.900±1.920 and 21.820±0.753%, respectively (Fig. 2E), consistent with the aforementioned TUNEL staining results. The results demonstrated that HG significantly increased the apoptotic rate of HUVECs compared with the NG group; however, apoptosis was significantly decreased in the HG+IQC treatment group compared with in the HG group (Fig. 2E).

Next, the protein expression levels of apoptotic markers, including Bax, Bcl-2 and C-caspase3, were analyzed. Compared with the cells treated with NG, western blotting analysis revealed that HG increased the protein levels of Bax and C-caspase3, and decreased the protein levels of Bcl-2, and these effects were attenuated by IQC treatment in a dose-dependent manner (Fig. 2C). Similarly, RT-qPCR results revealed that the change in the mRNA expression levels of Bax and Bcl-2 were consistent with those observed by western blotting analysis (Fig. 2D). Overall, the current results indicated that IQC may have a critical effect on HG-induced apoptosis of HUVECs.

IQC attenuates HG-induced apoptosis by regulating p53 in HUVECs. To investigate the underlying molecular mechanism of the effect of IQC on endothelial apoptosis, the effects of the p53 signaling pathway under HG stress in the absence or presence of IQC were explored. Western blotting results revealed that HG significantly induced p53 activation in HUVECs and that this effect was inhibited by IQC (Fig. 3A). Immunofluorescence staining indicated that HG exposure significantly enhanced p53 protein expression in the nucleus and that this effect was inhibited by IQC administration (Fig. 3B). To determine whether the protective effect of IQC was dependent on p53, cells were treated with a p53 inhibitor (pifithrin-β) or a p53-MDM2 antagonist (Nutlin-3) for 24 h. Next, the protein expression levels of p53, Bax, Bcl-2, and C-caspase 3 were measured. Under HG conditions, the protein levels of p53 and Bax were decreased, while the expression levels of Bcl-2 were increased in pifithrin-β-treated cells compared with the IQC-treated group (Fig. 3D). Meanwhile, Nutlin-3 and IQC co-treatment significantly increased the

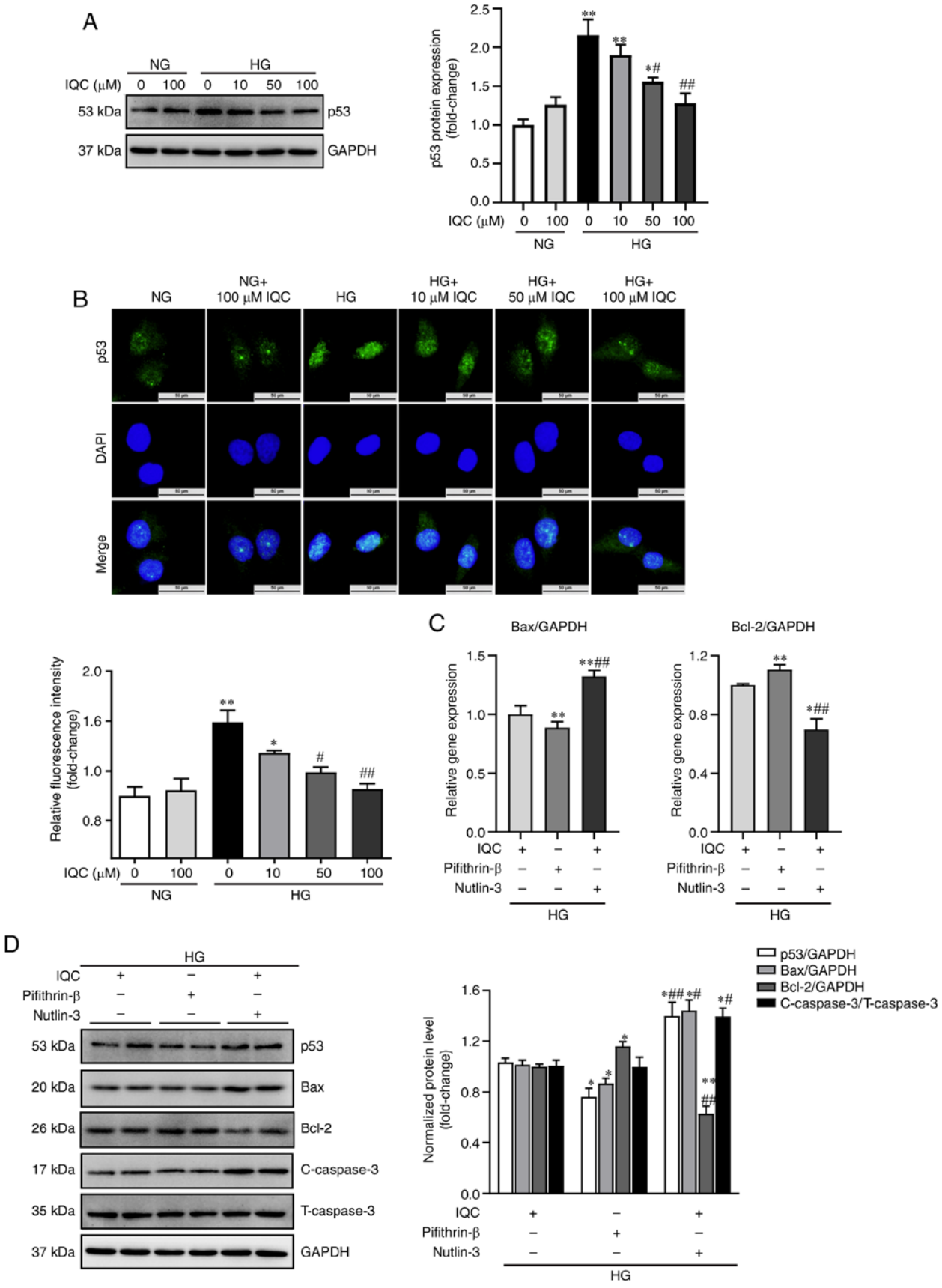

Figure 3. IQC attenuates HG-induced apoptosis by regulating p53. (A) Representative western blotting images of p53 protein bands and their quantification (n=3). GAPDH was used as a control. (B) Representative images and quantification of p53 expression examined by immunofluorescence staining. p53 (green); nucleus/DAPI (blue). Scale bar, 50 μm. *P<0.05 and **P<0.01 vs. NG. $^{\#}$P<0.05 and $^{\#\#}$P<0.01 vs. HG. (C) Relative mRNA expression levels of Bax and Bcl-2 in HUVECs treated with IQC, pifithrin-β alone or IQC plus Nutlin-3 under HG conditions (n=6). GAPDH was used as a control. (D) Representative western blotting images of p53, Bax, Bcl-2, C-caspase3, T-caspase3 and GAPDH protein bands in HUVECs treated with IQC, pifithrin-β alone or IQC plus Nutlin-3 under HG conditions, and their quantification (n=6). GAPDH was used as a control. *P<0.05 and **P<0.01 vs. IQC. $^{\#}$P<0.05 and $^{\#\#}$P<0.01 vs. pifithrin-β. NG, normal glucose; HG, high glucose; IQC, isoquercitrin; HUVECs, human umbilical vein endothelial cells; C/T-caspase 3, cleaved/total caspase 3.

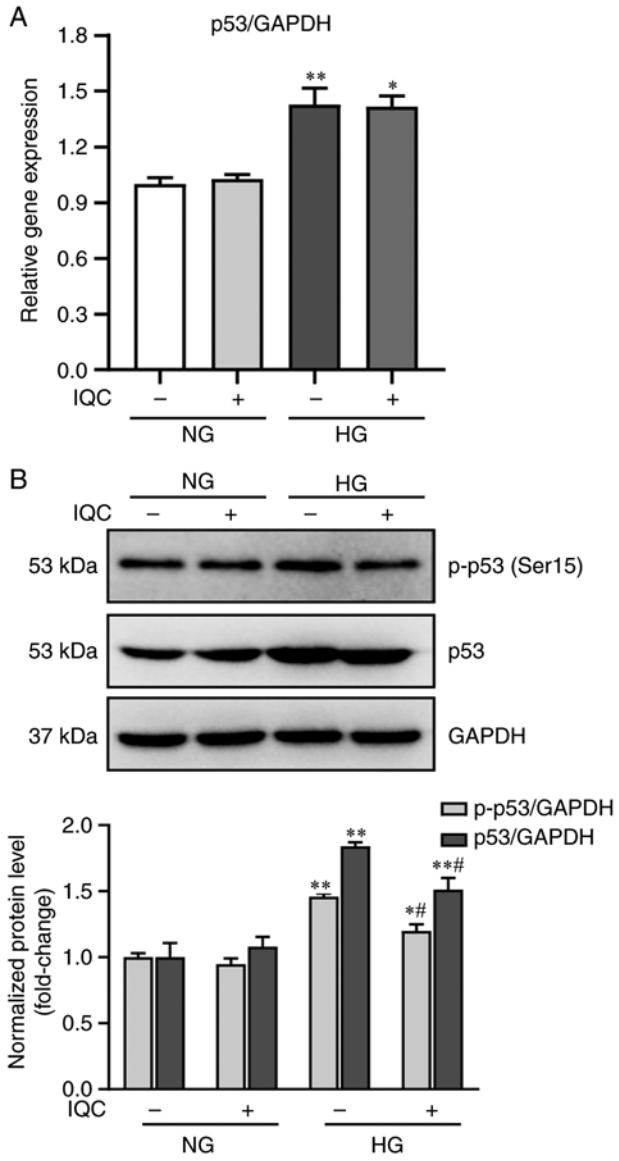

Figure 4. IQC inhibits the HG-induced phosphorylation of p53 at Ser15. (A) Relative mRNA expression levels of p53 in the indicated groups (n=6). GAPDH was used as a control. (B) Representative western blotting images of p-p53 (Ser15), p53 and GAPDH protein bands and their quantification (n=6). *P<0.05 and **P<0.01 vs. NG. #P<0.05 vs. HG. NG, normal glucose; HG, high glucose; IQC, isoquercitrin; p, phosphorylated.

protein expression levels of p53, Bax and C-caspase 3, and decreased Bcl-2 expression compared with in the IQC group under HG conditions (Fig. 3D). Similar trends were observed from the RT-qPCR results for Bax and Bcl-2 mRNA expression (Fig. 3C). Overall, the current results suggested that IQC partially attenuated HG-induced apoptosis of endothelial cells in a p53-dependent manner.

IQC exhibits a protective effect by regulating the post-translational modification of p53. As shown in Fig. 4A, IQC did not affect the mRNA expression levels of p53 in response to HG, indicating that IQC may control p53 expression by modulating p53 protein stability. Since phosphorylation is a well-known post-translational modification that regulates p53 stability, the phosphorylation of p53 was examined. Western blotting results revealed that p53 and p-p53 (Ser15) protein

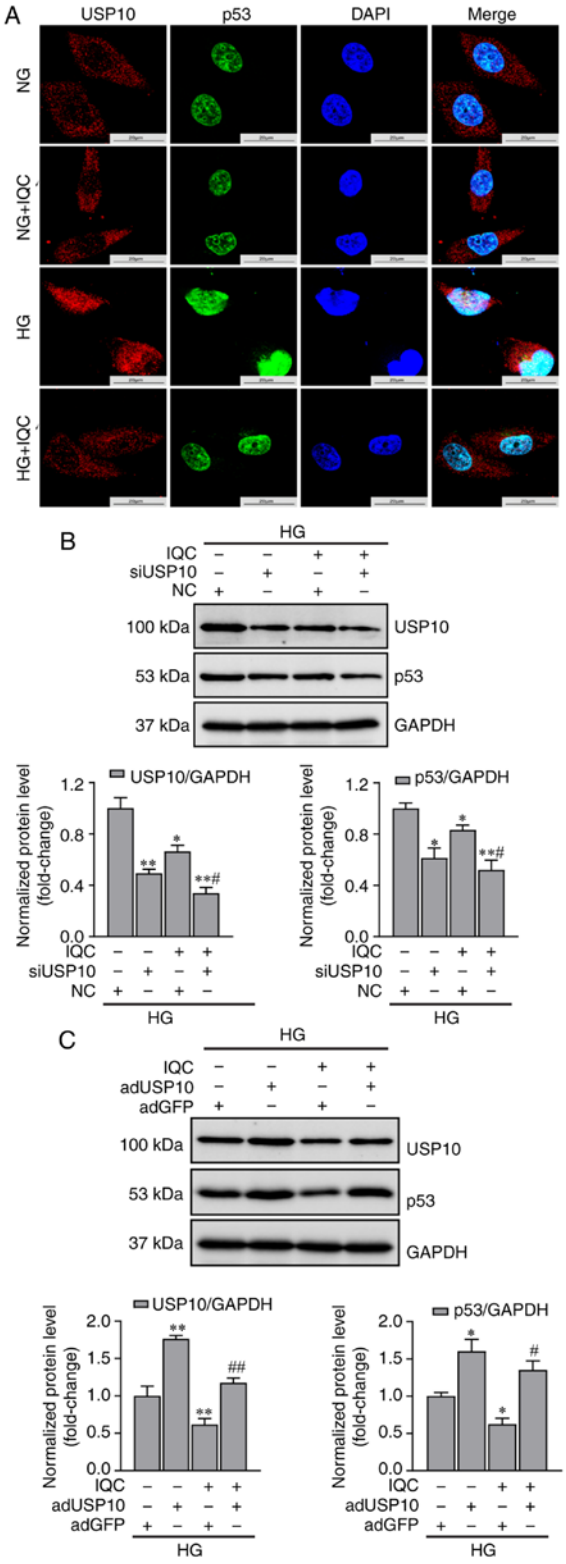

Figure 5. USP10 regulates the levels of p53 in IQC-treated cells under HG stress. (A) Representative immunofluorescence images of p53 and USP10 co-localization. Fluorescence was evaluated by confocal microscopy. p53 (green), USP10 (red), DAPI (blue). Scale bar, 20 μm. (B) Representative western blotting images of p53, USP10 and GAPDH protein bands in HUVECs transfected with siUSP10 or NC siRNA and their quantification (n=3). (C) Representative western blotting images of USP10, p53 and GAPDH protein bands in HUVECs infected with adUSP10 or adGFP and their quantification (n=3). *P<0.05 and **P<0.01 vs. NC or adGFP. #P<0.05 and ##P<0.01 vs. IQC+NC or IQC+adGFP. NG, normal glucose; HG, high glucose; IQC, isoquercitrin; HUVECs, human umbilical vein endothelial cells; si, small interfering; NC, negative control; USP10, ubiquitin specific peptidase 10; ad, adenovirus.

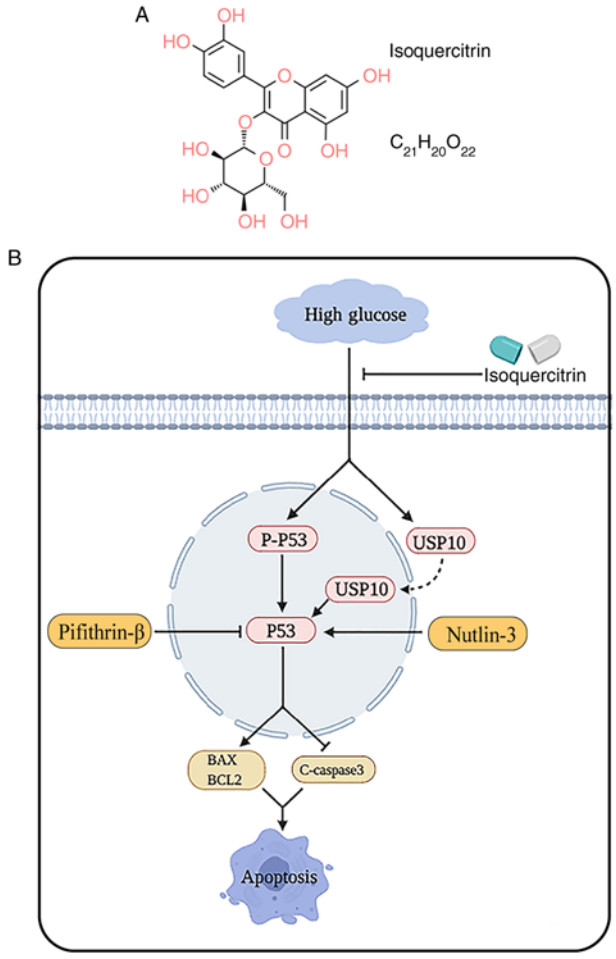

Figure 6. Chemical structure of isoquercitrin and the proposed mechanisms of the protective effect of isoquercitrin in endothelial cells. (A) Structure of isoquercitrin. (B) Isoquercitrin modulates HG-induced apoptosis through a p53-medicated signaling pathway in endothelial cells. USP10, ubiquitin specific peptidase 10; p, phosphorylated; C-caspase 3, cleaved caspase 3.

expression was significantly enhanced in the HG group compared with in the NG group. IQC treatment partially suppressed their expression levels under HG conditions compared with those in the HG group (Fig. 4B). In addition to phosphorylation, ubiquitination is involved in p53 protein stability, and it has been proven that USP10, an enzyme that mediates the deubiquitination of p53, specifically participates in the proteasomal degradation of p53 (24). Subsequently, the interaction between p53 and USP10 was demonstrated using immunofluorescence co-localization. Immunofluorescence images revealed that HG caused USP10 to translocate into the nucleus, while IQC treatment promoted the nuclear export of USP10 (Fig. 5A). Moreover, p53 expression in the nucleus was increased under HG stress, which was consistent with the findings shown in Fig. 3B.

To further confirm that the change in p53 expression induced by IQC was dependent on USP10, USP10 siRNA and adUSP10 were used to knock down and overexpress USP10, respectively. As shown in Fig. 5B, USP10 silencing significantly decreased p53 and USP10 protein expression in the siUSP10 group compared with that in the control group, and IQC treatment caused a further decrease in their expression levels in USP10-silenced HUVECs. By contrast, USP10 overexpression significantly promoted the HG-induced expression levels of USP10 and p53, and IQC treatment in adUSP10 HUVECs upregulated their expression levels compared with in the adGFP+IQC group (Fig. 5C).

Overall, the current results indicated that IQC exhibited a protective effect by regulating the phosphorylation of p53 and the nuclear export of USP10 in HG-induced apoptosis.

Discussion

DM can cause serious vascular complications due to the persistent damage of hyperglycemia to the endothelium (25). Moreover, it has been shown that HG induces the apoptosis of endothelial cells (ECs), and the loss of ECs further worsens endothelial function (8,26). Mounting evidence has demonstrated that promoting endothelial survival markedly alleviates vascular dysfunction induced by DM (3,27). In the present study, it was revealed that IQC decreased HG-induced apoptosis of HUVECs in a dose-dependent manner, suggesting that IQC may be used as a potential therapeutic strategy to protect blood vessels against HG stimulation. IQC (Fig. 6A), also named quercetin-3-O-b-D-glucopyranoside, is present in a broad range of natural plants, medicinal herbs, vegetables and fruits (12). IQC belongs to the bioflavonoid family and possesses pleiotropic biological effects under physiological and pathological conditions (13,28,29). Previous studies have shown that IQC has a neuroprotective effect by inhibiting neuronal apoptosis either in streptozotocin-induced neurotoxicity (30) or in cerebral ischemia/reperfusion injury (31). In addition to nerve cells, IQC has been proven to exert an anti-apoptotic effect in cardiomyocytes (14). Similarly, the present study confirmed that IQC exhibited anti-apoptotic effects in ECs in response to HG.

Apoptosis, also known as programmed cell death, is regulated by a complicated signaling network, and numerous proteins involved in different signaling pathways, such as TNF, Bax, Bcl-2, Caspase3 and Fas/FasL, have been confirmed to participate in this process (32). Among these proteins, p53 has been well documented to regulate apoptosis. p53 is a well-known tumor suppressor protein due to its powerful ability to promote cell cycle arrest or apoptosis in tumor cells (33). In addition to suppressing abnormal tumor cells, p53 participates in controlling the apoptosis of normal cells (34). Since p53 is an important regulator of apoptosis, p53 expression was examined in the present study in the absence or presence of HG. The current results revealed that HG increased the protein and mRNA expression levels of p53 in HUVECs, which is consistent with previous studies (35,36). In contrast to its beneficial role against tumors, p53 overexpression may be detrimental to ECs exposed to HG. A number of studies have reported that inhibiting the HG-induced increase in p53 significantly decreases apoptosis in ECs (37,38). In a type 2 diabetic mouse model, inhibition or downregulation of p53 attenuated coronary endothelial cell apoptosis, thus improving coronary flow velocity reserve and cardiac function (39). Additionally, p53 downregulation mediated by inhibiting early growth response gene-1 decreases HG-induced apoptosis and tube formation in human retinal vascular endothelial cells (40). In accordance with previous studies (41-43), the present study demonstrated that the potent p53 inhibitor pifithrin-β effectively attenuated

HG-induced apoptosis in HUVECs. Furthermore, it was revealed that IQC markedly decreased p53 expression induced by HG, and this effect was associated with the ability of IQC to decrease apoptosis, since activating p53 by Nutlin-3 blunted the anti-apoptotic effects of IQC in response to HG. A previous study has confirmed the potent anti-apoptotic effect of IQC by demonstrating that it attenuates the hydrogen peroxide-induced upregulation of p53 expression (44). Additionally, a network pharmacology analysis revealed that IQC has synergistic interactions with the p53 signaling pathway through apoptosis (45). The current data further demonstrated that IQC exerted its protective effect in ECs stimulated with HG by regulating p53.

p53 expression is regulated by a number of factors, such as USP10, RNA-binding motif protein 10 and suppressor of cytokine signaling 1, and the increase in intracellular p53 protein is mainly due to either increased p53 protein synthesis or decreased p53 protein degradation (46,47). In the present study, HG increased the mRNA expression levels of p53, indicating that it promoted the synthesis of p53 protein. Notably, it was revealed that IQC did not affect p53 mRNA expression in the absence or presence of HG, suggesting that IQC may regulate p53 protein expression by activating the p53 protein degradation pathway. It has been reported that various post-translational modifications, such as phosphorylation and ubiquitination, are involved in the proteasomal degradation process of the p53 protein, thus affecting p53 stability (48). A previous study indicated that HG induces the phosphorylation of p53 at Thr55 in ECs, leading to apoptosis (37). In addition, the current results revealed that HG increased the phosphorylation level of p53 at Ser15. It has been well documented that phosphorylation at Ser15 weakens the interaction between p53 and MDM2 (49). MDM2 is a negative regulator of p53 that binds to p53 and promotes its ubiquitination and proteasomal degradation (50). Phosphorylation of p53 at Ser15 improves its stability and activity. Therefore, HG may promote the production of p53, as well as enhance its stability. Since IQC regulated p53 protein expression rather than mRNA expression, the present study measured the phosphorylation level of p53 at Ser15 in HUVECs. The current results revealed that IQC markedly decreased the HG-induced phosphorylation of p53 at Ser15, suggesting that IQC may promote p53 proteasomal degradation by regulating p53 phosphorylation levels.

In contrast to phosphorylation, which promotes p53 stability, ubiquitination enhances the proteasomal degradation of p53; thus, deubiquitination is another important regulatory mechanism for maintaining the stability of p53 (51). USP10 is a newly discovered deubiquitinase that can remove ubiquitin from p53 to promote its stability (52,53). It should be noted that MDM2 is also the major E3 ubiquitin ligase of p53 (54). USP10 acts primarily on p53 but does not affect MDM2 activity or MDM2 binding with p53 (52). However, the role of USP10 in response to HG is unknown. Thus, USP10 expression was evaluated in the present study. The data indicated that HG resulted in the nuclear translocation of USP10 and its subsequent binding to p53, thus promoting the stability of p53, and this effect was partially blunted in IQC-treated HUVECs. Moreover, using siRNA and adUSP10 to silence and overexpress USP10 in HUVECs under HG stress, respectively, it was revealed that the protective effect of IQC mediated by its regulation of p53 levels may be dependent on USP10. Currently, it has been proven that IQC is involved in regulating the ubiquitin-proteasome system, but the molecular mechanism remains unclear (55). The present study suggested that IQC may affect p53 expression by regulating intercellular USP10 localization, suggesting that USP10 may be one of the targets of IQC.

In conclusion, the present study demonstrated that IQC effectively alleviated HG-induced apoptosis in HUVECs (Fig. 6B). Moreover, it was revealed that the anti-apoptotic effects of IQC may occur via modulation of p53 post-transcriptional modification rather than suppression of p53 protein synthesis. IQC inhibited the HG-induced phosphorylation of p53 at Ser15 and increased the nuclear transport of USP10, thereby increasing the proteasomal degradation of the p53 protein in HG-treated HUVECs. Thus, using IQC to affect p53 stability may be a potential therapeutic strategy for vascular complications induced by DM.

Acknowledgements

Not applicable.

Funding

The present study was supported by the National Natural Science Foundation of China (grant no. 81530012), the Fundamental Research Funds for the Central Universities (grant nos. 2042020kf0052 and 2042018kf1032), the National Key R&D Program of China (grant no. 2018YFC1311300), the Development Center for Medical Science and Technology National Health and Family Planning Commission of the People's Republic of China (The prevention and control project of cardiovascular disease; grant no. 2016ZX-008-01) and the Science and Technology Planning Projects of Wuhan (grant no. 2018061005132295).

Availability of data and materials

The datasets used and/or analyzed during the current study are available from the corresponding author on reasonable request.

Authors' contributions

LL, SH, MX and QT contributed to the conception and design of the study. LL, SH, HW and MX analyzed the data. DL and CW established the cellular model. LL, SH, HW and YG performed the experiments and participated in data acquisition. LL and SH drafted the manuscript. YG and QT revised the manuscript. LL, SH, MX, HW and QT confirmed the authenticity of all the raw data. All authors read and approved the final manuscript.

Ethics approval and consent to participate

Not applicable.

Patient consent for publication

Not applicable.

Competing interests

The authors declare that they have no competing interests.

References

1. Schmidt AM: Highlighting diabetes mellitus: The epidemic continues. Arterioscler Thromb Vasc Biol 38: e1-e8, 2018.
2. Eelen G, de Zeeuw P, Simons M and Carmeliet P: Endothelial cell metabolism in normal and diseased vasculature. Circ Res 116: 1231-1244, 2015.
3. Yu S, Liu X, Men L, Yao J, Xing Q and Du J: Selenoprotein S protects against high glucose-induced vascular endothelial apoptosis through the PKCβII/JNK/Bcl-2 pathway. J Cell Biochem, Nov 28, 2018 (Online ahead of print).
4. Watson EC, Grant ZL and Coultas L: Endothelial cell apoptosis in angiogenesis and vessel regression. Cell Mol Life Sci 74: 4387-4403, 2017.
5. Zhang Y, Lv X, Hu Z, Ye X, Zheng X, Ding Y, Xie P and Liu Q: Protection of Mcc950 against high-glucose-induced human retinal endothelial cell dysfunction. Cell Death Dis 8: e2941, 2017.
6. Han X, Wang B, Sun Y, Huang J, Wang X, Ma W, Zhu Y, Xu R, Jin H and Liu N: Metformin modulates high glucose-incubated human umbilical vein endothelial cells proliferation and apoptosis through AMPK/CREB/BDNF pathway. Front Pharmacol 9: 1266, 2018.
7. Gu J, Huang W, Zhang W, Zhao T, Gao C, Gan W, Rao M, Chen Q, Guo M, Xu Y and Xu YH: Sodium butyrate alleviates high-glucose-induced renal glomerular endothelial cells damage via inhibiting pyroptosis. Int Immunopharmacol 75: 105832, 2019.
8. Zhao X, Su L, He X, Zhao B and Miao J: Long noncoding RNA CA7-4 promotes autophagy and apoptosis via sponging MIR877-3P and MIR5680 in high glucose-induced vascular endothelial cells. Autophagy 16: 70-85, 2020.
9. Ko YS, Jin H, Park SW and Kim HJ: Salvianolic acid B protects against oxLDL-induced endothelial dysfunction under high-glucose conditions by downregulating ROCK1-mediated mitophagy and apoptosis. Biochem Pharmacol 174: 113815, 2020.
10. Wei H, Cao C, Wei X, Meng M, Wu B, Meng L, Wei X, Gu S and Li H: Circular RNA circVEGFC accelerates high glucose-induced vascular endothelial cells apoptosis through miR-338-3p/HIF-1α/VEGFA axis. Aging (Albany NY) 12: 14365-14375, 2020.
11. Yi J and Gao ZF: MicroRNA-9-5p promotes angiogenesis but inhibits apoptosis and inflammation of high glucose-induced injury in human umbilical vascular endothelial cells by targeting CXCR4. Int J Biol Macromol 130: 1-9, 2019.
12. Valentová K, Vrba J, Bancířová M, Ulrichová J and Křen V: Isoquercitrin: Pharmacology, toxicology, and metabolism. Food Chem Toxicol 68: 267-282, 2014.
13. Huang SH, Xu M, Wu HM, Wan CX, Wang HB, Wu QQ, Liao HH, Deng W and Tang QZ: Isoquercitrin attenuated cardiac dysfunction via AMPKα-dependent pathways in LPS-treated mice. Mol Nutr Food Res 62: e1800955, 2018.
14. Ma C, Jiang Y, Zhang X, Chen X, Liu Z and Tian X: Isoquercetin ameliorates myocardial infarction through anti-inflammation and anti-apoptosis factor and regulating TLR4-NF-κB signal pathway. Mol Med Rep 17: 6675-6680, 2018.
15. Gasparotto Junior A, Dos Reis Piornedo R, Assreuy J and Da Silva-Santos JE: Nitric oxide and Kir6.1 potassium channel mediate isoquercitrin-induced endothelium-dependent and independent vasodilation in the mesenteric arterial bed of rats. Eur J Pharmacol 788: 328-334, 2016.
16. Bondonno NP, Bondonno CP, Ward NC, Woodman RJ, Hodgson JM and Croft KD: Enzymatically modified isoquercitrin improves endothelial function in volunteers at risk of cardiovascular disease. Br J Nutr 123: 182-189, 2020.
17. Jayachandran M, Wu Z, Ganesan K, Khalid S, Chung SM and Xu B: Isoquercetin upregulates antioxidant genes, suppresses inflammatory cytokines and regulates AMPK pathway in streptozotocin-induced diabetic rats. Chem Biol Interact 303: 62-69, 2019.
18. Niu C, Chen Z, Kim KT, Sun J, Xue M, Chen G, Li S, Shen Y, Zhu Z, Wang X, *et al*: Metformin alleviates hyperglycemia-induced endothelial impairment by downregulating autophagy via the hedgehog pathway. Autophagy 15: 843-870, 2019.
19. Yu L, Liang Q, Zhang W, Liao M, Wen M, Zhan B, Bao H and Cheng X: HSP22 suppresses diabetes-induced endothelial injury by inhibiting mitochondrial reactive oxygen species formation. Redox Biol 21: 101095, 2019.
20. Liu J, Meng Z, Gan L, Guo R, Gao J, Liu C, Zhu D, Liu D, Zhang L, Zhang Z, *et al*: C1q/TNF-related protein 5 contributes to diabetic vascular endothelium dysfunction through promoting Nox-1 signaling. Redox Biol 34: 101476, 2020.
21. Christodoulou MS, Colombo F, Passarella D, Ieronimo G, Zuco V, De Cesare M and Zunino F: Synthesis and biological evaluation of imidazolo(2,1-b)benzothiazole derivatives, as potential p53 inhibitors. Bioorg Med Chem 19: 1649-1657, 2011.
22. Zhang Y, Zhang Q, Zeng SX, Zhang Y, Mayo LD and Lu H: Inauhzin and Nutlin3 synergistically activate p53 and suppress tumor growth. Cancer Biol Ther 13: 915-924, 2012.
23. Livak KJ and Schmittgen TD: Analysis of relative gene expression data using real-time quantitative PCR and the 2(-Delta Delta C(T)) method. Methods 25: 402-408, 2001.
24. Kwon SK, Saindane M and Baek KH: p53 stability is regulated by diverse deubiquitinating enzymes. Biochim Biophys Acta Rev Cancer 1868: 404-411, 2017.
25. Domingueti CP, Dusse LM, Carvalho MD, de Sousa LP, Gomes KB and Fernandes AP: Diabetes mellitus: The linkage between oxidative stress, inflammation, hypercoagulability and vascular complications. J Diabetes Complications 30: 738-745, 2016.
26. Elshaer SL, Lemtalsi T and El-Remessy AB: High glucose-mediated tyrosine nitration of PI3-Kinase: A molecular switch of survival and apoptosis in endothelial cells. Antioxidants (Basel) 7: 47, 2018.
27. Liu C, Yao MD, Li CP, Shan K, Yang H, Wang JJ, Liu B, Li XM, Yao J, Jiang Q and Yan B: Silencing of circular RNA-ZNF609 ameliorates vascular endothelial dysfunction. Theranostics 7: 2863-2877, 2017.
28. Kim JH, Lee S and Cho EJ: The protective effects of acer okamotoanum and Isoquercitrin on obesity and amyloidosis in a mouse model. Nutrients 12: 1353, 2020.
29. Resham K, Khare P, Bishnoi M and Sharma SS: Neuroprotective effects of isoquercitrin in diabetic neuropathy via Wnt/β-catenin signaling pathway inhibition. Biofactors 46: 411-420, 2020.
30. Chen L, Feng P, Peng A, Qiu X, Lai W, Zhang L and Li W: Protective effects of isoquercitrin on streptozotocin-induced neurotoxicity. J Cell Mol Med 24: 10458-10467, 2020.
31. Dai Y, Zhang H, Zhang J and Yan M: Isoquercetin attenuates oxidative stress and neuronal apoptosis after ischemia/reperfusion injury via Nrf2-mediated inhibition of the NOX4/ROS/NF-κB pathway. Chem Biol Interact 284: 32-40, 2018.
32. Dong Y, Chen H, Gao J, Liu Y, Li J and Wang J: Molecular machinery and interplay of apoptosis and autophagy in coronary heart disease. J Mol Cell Cardiol 136: 27-41, 2019.
33. Bykov VJ, Issaeva N, Shilov A, Hultcrantz M, Pugacheva E, Chumakov P, Bergman J, Wiman KG and Selivanova G: Restoration of the tumor suppressor function to mutant p53 by a low-molecular-weight compound. Nat Med 8: 282-288, 2002.
34. Gao Y, Yin H, Zhang Y, Dong Y, Yang F, Wu X and Liu H: Dexmedetomidine protects hippocampal neurons against hypoxia/reoxygenation-induced apoptosis through activation HIF-1α/p53 signaling. Life Sci 232: 116611, 2019.
35. Schisano B, Tripathi G, McGee K, McTernan PG and Ceriello A: Glucose oscillations, more than constant high glucose, induce p53 activation and a metabolic memory in human endothelial cells. Diabetologia 54: 1219-1226, 2011.
36. Li Q, Pang L, Shi H, Yang W, Liu X, Su G and Dong Y: High glucose concentration induces retinal endothelial cell apoptosis by activating p53 signaling pathway. Int J Clin Exp Pathol 11: 2401-2407, 2018.
37. Wu Y, Lee S, Bobadilla S, Duan SZ and Liu X: High glucose-induced p53 phosphorylation contributes to impairment of endothelial antioxidant system. Biochim Biophys Acta Mol Basis Dis 1863: 2355-2362, 2017.
38. Chan WH and Wu HJ: Methylglyoxal and high glucose co-treatment induces apoptosis or necrosis in human umbilical vein endothelial cells. J Cell Biochem 103: 1144-1157, 2008.
39. Si R, Zhang Q, Tsuji-Hosokawa A, Watanabe M, Willson C, Lai N, Wang J, Dai A, Scott BT, Dillmann WH, *et al*: Overexpression of p53 due to excess protein O-GlcNAcylation is associated with coronary microvascular disease in type 2 diabetes. Cardiovasc Res 116: 1186-1198, 2020.
40. Ao H, Liu B, Li H and Lu L: Egr1 mediates retinal vascular dysfunction in diabetes mellitus via promoting p53 transcription. J Cell Mol Med 23: 3345-3356, 2019.

41. Da Pozzo E, La Pietra V, Cosimelli B, Da Settimo F, Giacomelli C, Marinelli L, Martini C, Novellino E, Taliani S and Greco G: p53 functional inhibitors behaving like pifithrin-β counteract the Alzheimer peptide non-β-amyloid component effects in human SH-SY5Y cells. ACS Chem Neurosci 5: 390-399, 2014.
42. Chen DZ, Wang WW, Chen YL, Yang XF, Zhao M and Yang YY: miR-128 is upregulated in epilepsy and promotes apoptosis through the SIRT1 cascade. Int J Mol Med 44: 694-704, 2019.
43. Kelly RM, Goren EM, Taylor PA, Mueller SN, Stefanski HE, Osborn MJ, Scott HS, Komarova EA, Gudkov AV, Holländer GA and Blazar BR: Short-term inhibition of p53 combined with keratinocyte growth factor improves thymic epithelial cell recovery and enhances T-cell reconstitution after murine bone marrow transplantation. Blood 115: 1088-1097, 2010.
44. Jung SH, Kim BJ, Lee EH and Osborne NN: Isoquercitrin is the most effective antioxidant in the plant Thuja orientalis and able to counteract oxidative-induced damage to a transformed cell line (RGC-5 cells). Neurochem Int 57: 713-721, 2010.
45. Taha KF, Khalil M, Abubakr MS and Shawky E: Identifying cancer-related molecular targets of Nandina domestica Thunb. by network pharmacology-based analysis in combination with chemical profiling and molecular docking studies. J Ethnopharmacol 249: 112413, 2020.
46. Jung JH, Lee H, Zeng SX and Lu H: RBM10, a new regulator of p53. Cells 9: 2107, 2020.
47. Saint-Germain E, Mignacca L, Vernier M, Bobbala D, Ilangumaran S and Ferbeyre G: SOCS1 regulates senescence and ferroptosis by modulating the expression of p53 target genes. Aging (Albany NY) 9: 2137-2162, 2017.
48. Liu Y, Tavana O and Gu W: p53 modifications: Exquisite decorations of the powerful guardian. J Mol Cell Biol 11: 564-577, 2019.
49. Shieh SY, Ikeda M, Taya Y and Prives C: DNA damage-induced phosphorylation of p53 alleviates inhibition by MDM2. Cell 91: 325-334, 1997.
50. Momand J, Zambetti GP, Olson DC, George D and Levine AJ: The mdm-2 oncogene product forms a complex with the p53 protein and inhibits p53-mediated transactivation. Cell 69: 1237-1245, 1992.
51. Liu J, Xia H, Kim M, Xu L, Li Y, Zhang L, Cai Y, Norberg HV, Zhang T, Furuya T, *et al*: Beclin1 controls the levels of p53 by regulating the deubiquitination activity of USP10 and USP13. Cell 147: 223-234, 2011.
52. Yuan J, Luo K, Zhang L, Cheville JC and Lou Z: USP10 regulates p53 localization and stability by deubiquitinating p53. Cell 140: 384-396, 2010.
53. Deng CC, Zhu DH, Chen YJ, Huang TY, Peng Y, Liu SY, Lu P, Xue YH, Xu YP, Yang B and Rong Z: TRAF4 promotes fibroblast proliferation in keloids by destabilizing p53 via interacting with the deubiquitinase USP10. J Invest Dermatol 139: 1925-1935.e5, 2019.
54. Honda R, Tanaka H and Yasuda H: Oncoprotein MDM2 is a ubiquitin ligase E3 for tumor suppressor p53. FEBS Lett 420: 25-27, 1997.
55. Carmona V, Martín-Aragón S, Goldberg J, Schubert D and Bermejo-Bescós P: Several targets involved in Alzheimer's disease amyloidogenesis are affected by morin and isoquercitrin. Nutr Neurosci 23: 575-590, 2020.

This work is licensed under a Creative Commons Attribution-NonCommercial-NoDerivatives 4.0 International (CC BY-NC-ND 4.0) License.